Journal of Theoretical Biology 571 (2023) 111561

Contents lists available at ScienceDirect

Journal of Theoretical Biology

journal homepage: www.elsevier.com/locate/yjtbi

A mathematical study of the efficacy of possible negative feedback pathways involved in neuronal polarization

Fan Bai [a], Richard Bertram [a,b,c], Bhargav R. Karamched [a,b,c,*]

[a] Department of Mathematics, Florida State University, Tallahassee FL 32306, United States
[b] Program in Molecular Biophysics, Florida State University, Tallahassee FL 32306, United States
[c] Program in Neuroscience, Florida State University, Tallahassee FL 32306, United States

ARTICLE INFO

Keywords:
Neuronal polarization
Bistability
Negative feedback
Stochastic dynamical system

ABSTRACT

Neuronal polarization, a process wherein nascent neurons develop a single long axon and multiple short dendrites, can occur within *in vitro* cell cultures without environmental cues. This is an apparently random process in which one of several short processes, called neurites, grows to become long, while the others remain short. In this study, we propose a minimum model for neurite growth, which involves bistability and random excitations reflecting actin waves. Positive feedback is needed to produce the bistability, while negative feedback is required to ensure that no more than one neurite wins the winner-takes-all contest. By applying the negative feedback to different aspects of the neurite growth process, we demonstrate that targeting the negative feedback to the excitation amplitude results in the most persistent polarization. Also, we demonstrate that there are optimal ranges of values for the neurite count, and for the excitation rate and amplitude that best maintain the polarization. Finally, we show that a previously published model for neuronal polarization based on competition for limited resources shares key features with our best-performing minimal model: bistability and negative feedback targeted to the size of random excitations.

1. Introduction

A nervous system is composed of interconnected neurons, each of which has multiple short dendrites that receive signals from upstream neurons and a single long axon that transmits signals to downstream neurons. Early in development, however, a neuron has multiple short neurites of similar lengths that extend and retract repeatedly and apparently randomly (coined by Dotti et al. (1988) as Stage 2). These neurites later differentiate into dendrites and a single axon (Fig. 1). The symmetry-breaking process by which a single axon emerges from the neurites (Stage 3) is referred to as *neuronal polarization*. Surprisingly, this process does not require release of growth factors from target cells, as neuronal polarization has been shown to occur within *in vitro* hippocampal neuron cell cultures in which there are no growth factor gradients guiding the selection process (Dotti et al., 1988; Wissner-Gross et al., 2013). The symmetry breaking appears to be random, and in experiments where the initial axon was cleaved off, a new one emerged from one of the other neurites (Goslin and Banker, 1989). Subsequent experimental manipulations demonstrated that it was possible for any neurite to become the winning neurite in the winner-takes-all contest (Takano et al., 2017a; Yamamoto et al., 2012). It has been shown that even in the *in vivo* setting where growth factor gradients are present, the developing neurons go through these stages, lasting about a day, characterized by growth and retraction of neurites with a subsequent symmetry breaking event (Tabata and Nakajima, 2003; Noctor et al., 2004). In this case, growth factor gradients influence the selection process, and indeed the random growth and retraction of neurites is thought to be a way for the neurites to explore the environment to seek out the growth factors (called *neurotrophins*). Nonetheless, even *in vivo* there is a winner-takes-all process that takes place, with bias provided by neurotrophin gradients.

There have been many studies aimed at understanding the biophysical mechanism of the neuronal polarization process (Inagaki et al., 2011; Banker, 2018; Takano et al., 2019, 2017a; Arimura and Kaibuchi, 2007; Winans et al., 2016; Yogev and Shen, 2017). Several potential mechanisms have been identified, and it is clear that the process involves positive feedback signals to promote the growth of the axon as well as negative feedback signals to prevent the emergence of a second axon (Fivaz et al., 2008; Namba et al., 2015; Takano et al., 2019; Toriyama et al., 2010; Yogev and Shen, 2017). In this article, we focus on the polarization process that occurs *in vitro*, without external neurotrophin gradients, using a minimal model for the winner-take-all selection process that incorporates positive feedback and explores the

* Correspondence to: LOV Building Rm 313, 1017 Academic Way, Tallahassee, FL 32306, United States
E-mail address: bkaramched@fsu.edu (B.R. Karamched).

https://doi.org/10.1016/j.jtbi.2023.111561
Received 1 March 2023; Received in revised form 29 May 2023; Accepted 11 June 2023
Available online 16 June 2023
0022-5193/Published by Elsevier Ltd.

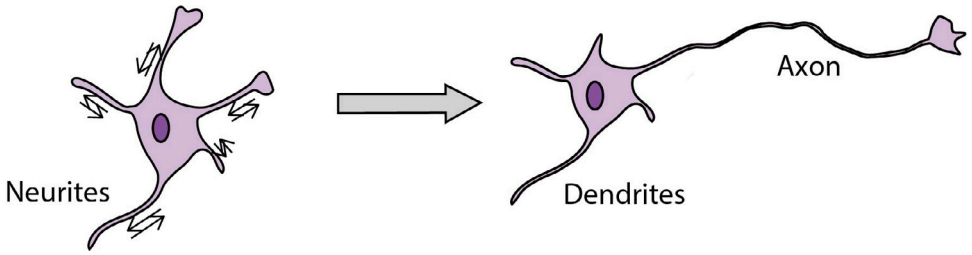

Fig. 1. Neuronal polarization. A nascent neuron (stage 2) has several short neurites that extend and retract repeatedly and randomly (left). Later, during stage 3, one of the neurites develops into an axon while others become dendrites (right).

efficacy of several different negative feedback mechanism in generating persistent neuronal polarization.

The model is constructed based on the hypothesis that the dynamics underlying neurite growth and retraction are such that the system is bistable. That is, each neurite has two stable equilibria, short and long. The bistability is a product of the positive feedback. A second hypothesis is that the selection process is truly random, so no neurite is biased towards winning the competition to become an axon. We then explore three mechanisms of negative feedback. One of these involves the retraction rate that is common to all neurites. The others involve a stochastic term that reflects randomly-timed and uniformly distributed actin waves which are known to be key to neurite elongation; each actin wave provides growth spurts by locally increasing the neurite volume to allow for microtubule polymerization (Winans et al., 2016; Inagaki and Katsuno, 2017a; Ruthel and Banker, 1999a). We consider the effects of making neurite retraction, actin wave magnitude, and actin wave frequency dependent on the combined length of the neurites such that increased length increases the retraction rate, or decreases the actin wave magnitude or frequency. In all cases, the negative feedback is unbiased.

The results demonstrate that targeting the negative feedback to the stochastic growth magnitude (i.e., the actin wave term) results in the most persistent polarized system. They also demonstrate that having more than 2 neurites, but less than some upper bound, is optimal for achieving and maintaining neuronal polarization. This is consistent with the finding that most nascent neurons have between 2 and 10 neurites (Wissner-Gross et al., 2013). One model for neuronal polarization is based on competition for limited resources, including growth factor (Toriyama et al., 2010). In the last section of Results, we demonstrate that a simplified model based on this limited-resource model contains the two elements that we find to be most successful at achieving persistent polarization: bistability and length-dependent reduction in the amplitude of actin-wave-driven stochastic excitation .

2. The minimal model

We consider a small population of R neurites, each with length L_i, $i = 1, 2, \ldots, R$. The basic model contains a term for positive feedback, a retraction term, and a stochastic term reflecting randomly-timed actin waves. The negative feedback is included later. The basic model is:

$$\frac{\mathrm{d}L_i}{\mathrm{d}t} = g\,\frac{L_i^2}{L_i^2 + K^2} - rL_i + \sum_n A\delta(t - t_n^{(i)}(\lambda)), \quad i = 1, 2, \ldots, R. \tag{1}$$

The first term reflects positive feedback through intracellular signaling (Arimura and Kaibuchi, 2007; Cheng et al., 2011; Inagaki et al., 2011; Takano et al., 2019; Namba et al., 2015; Yogev and Shen, 2017), length-dependent diffusion of polarity effectors (Schelski and Bradke, 2017; Toriyama et al., 2010; Naoki et al., 2011), and stabilization of microtubules (Gomis-Rüth et al., 2008; Farías et al., 2019). Positive feedback is an essential ingredient of bistability (Alon, 2020). The second term provides a constant rate of neurite retraction, reflecting the retraction that occurs in all neurites between the arrival of actin waves (Winans et al., 2016). The last term includes a sum of

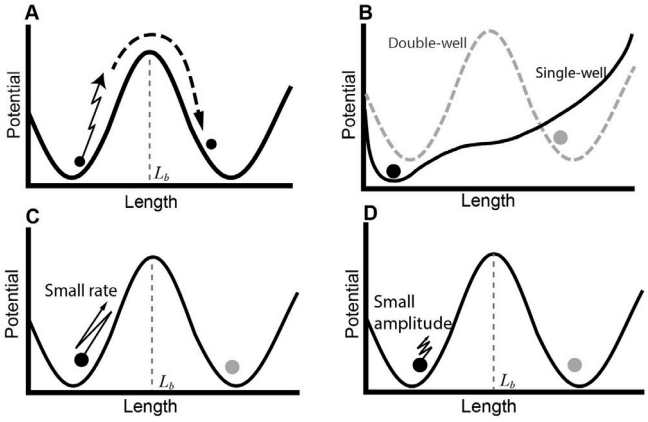

Fig. 2. The bistability in the neurite growth model interpreted as a double well potential and the effects of negative feedback. (A) The double well potential shows the bistability in neuronal polarization. Due to random excitations, a particle representing a neurite may cross the potential barrier, located at position L_b. (B) The increased retraction rate due to the formation of an axon (gray dot) destroys the double well potential for a short neurite (black dot). (C) Under the excitation rate reduction, the particle falls back significantly between two excitations. (D) Under the excitation amplitude reduction, each pulse only helps the particle climb a short distance.

delta functions that describes sudden neurite elongation due to actin waves (Winans et al., 2016; Inagaki and Katsuno, 2017b; Ruthel and Banker, 1999b). Each wave induces a jump in length of size A. The term $t_n^{(i)}(\lambda)$ is the time when the tip of the ith neurite receives the nth wave, which follows a Poisson process of rate λ (this is also the average number of waves generated per unit time).

With our minimal model, a neurite can be thought of as a particle in a double-well potential, as shown in Fig. 2A. The left potential well corresponds to the state of being a short neurite, and the right well corresponds to the state of being a long neurite that will become an axon. The actin waves then provide random excitations that can drive the particle across the potential barrier at location L_b, marking the establishment of an axon. All nascent neurons have short neurites, so they begin in the left potential well.

Since only one neurite develops into the axon of a typical neuron, the growth of other neurites should be suppressed to avoid having multiple axons. One way to incorporate this negative feedback into the model is to have the retraction rate r increase as the neurites get longer. For simplicity, we use the following length-dependent retraction rate:

$$r = r_0\left(1 + \alpha\sum_{i=1}^{R} L_i\right), \tag{2}$$

where r_0 is a basal retraction rate and α is a parameter that controls the degree of suppression. The retraction rate is the same for every neurite, so the suppression is unbiased. Reducing the growth rate g in an unbiased way will give qualitatively similar results. Targeting the negative feedback to the retraction rate has the effect of eliminating the upper equilibrium state for each of the short neurites (Fig. 2B).

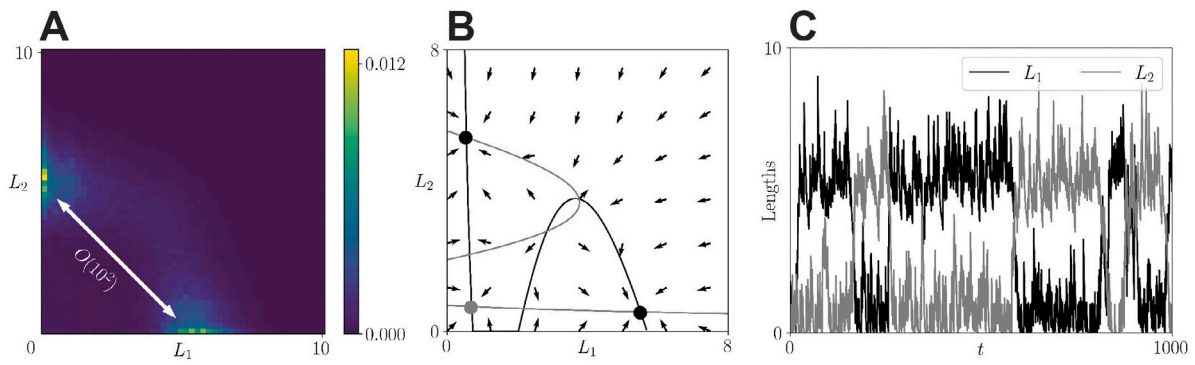

Fig. 3. The dynamics of the two-neurite system when negative feedback targets the retraction rate. (A) The long-term probability density of the neurite lengths exhibits two peaks. The mean transition time between the peaks is of $O(10^2)$, which is estimated by the mean time to enter $[4,8]\times[0,2]$ from $(0,6)$. (B) The phase portrait of Eq. (5) shows two stable equilibria close to the peaks of the stationary probability density, corresponding to two polarized states. The L_1-nullclines (black) and L_2-nullclines (gray) intersect at 5 additional locations, one of which (gray point) is a stable equilibrium. (C) Monte Carlo simulation shows frequent alternations in the lengths of neurite 1 (black) and neurite 2 (gray). To study the effect of the increased retraction alone, we set $\lambda = \lambda_0$ and $A = A_0$. Other parameter values are given in Table 1.

Biologically, the increased retraction rate reflects the collection of inhibitory signals in the cell body sent from the neurite tips.

Since actin waves drive neurite growth, negative feedback can also be implemented by suppressing the generation of the waves. In our model, this is done by reducing the excitation rate λ according to the following equation:

$$\lambda = \frac{\lambda_0}{1+\mu\sum_{i=1}^{R} L_i}, \tag{3}$$

where λ_0 is a basal excitation rate and μ controls the degree of reduction. Again, the inhibition is unbiased because the actin waves are shared equally among neurites. Under the rate reduction, a neurite retracts significantly between two waves, so its net growth is small (Fig. 2C). A length-dependent decrease in actin wave frequency is consistent with the observation that actin waves are less frequent once an axon is formed (Ruthel and Banker, 1999a). This inhibitory mechanism was also implemented in a previous mathematical model (Naoki et al., 2011; Naoki and Ishii, 2014).

Finally, we implement negative feedback by reducing the amplitude A as follows:

$$A = \frac{A_0}{1+\phi\sum_{i=1}^{R} L_i}, \tag{4}$$

where A_0 is a basal excitation amplitude and ϕ controls the degree of reduction. In terms of the particle in a double well potential, a reduced amplitude means that more excitations will be required to cross the potential barrier (Fig. 2D). Biologically, actin waves carry growth factors produced at the cell body, so amplitude reduction could reflect depletion of the growth factors. A similar amplitude reduction mechanism was adopted in a previous modeling study (Toriyama et al., 2010).

3. Persistence of polarization with different forms of negative feedback

For mathematical simplicity, we consider a nascent neuron with two neurites ($R = 2$) in this section. In fact, neurons with two neurites were also observed in experiments (Wissner-Gross et al., 2013). For such a neuron, we study the effect of each of the three negative feedback mechanisms from three perspectives: (1) the joint probability density of the lengths, denoted by $p(L_1, L_2)$, (2) the underlying deterministic phase portraits, and (3) the stochastic dynamics. To analyze the probability density and stochastic dynamics, we employ two complementary methods: the generalized cell-mapping method (GCM) and Monte Carlo (MC) simulations, which are explained in detail in Appendix. The GCM allows us to efficiently determine the probability density of the lengths and its long-term limit. However, when dealing with neurons possessing more than two neurites, the GCM becomes computationally expensive. In such cases, the MC method proves to be more efficient, particularly when the timescale is short. Additionally, the MC method unveils neurite dynamics that are not captured by the probability density obtained through the GCM. Nevertheless, the MC method is less effective than the GCM in analyzing the long-term behavior of the probability density.

Table 1
List of parameters and their values used in the study of different negative feedback mechanisms.

Notation	Definition	Value
g	Maximum growth rate	10
K	Half activation level	$\sqrt{21}$
r_0	Basal retraction rate	1
α	Feedback coefficient of increased retraction	0.026
λ_0	Basal excitation rate	1
μ	Feedback coefficient of reduced excitation rate	0.4
A_0	Basal excitation amplitude	1
ϕ	Feedback coefficient of reduced excitation amplitude	0.4
L_b	Location of the potential barrier	3

We begin by considering negative feedback through a length-dependent increase in the neurite retraction rate (Eq. (2)). The long-term joint probability distribution of the lengths exhibits two peaks, which indicates that the system spends most of the time near these peaks (Fig. 3A). Each peak represents a state with a long neurite and a short neurite, which we refer to as a *polarized state*. The formation of the peaks can be inferred from the following deterministic system:

$$\frac{\mathrm{d}L_i}{\mathrm{d}t} = g\frac{L_i^2}{L_i^2+K^2} - rL_i + \frac{1}{2}A\lambda, \quad i = 1,2, \tag{5}$$

where the term $\frac{1}{2}A\lambda$ is the time average of the Poissonian term in Eq. (1). The factor $1/2$ accounts for the fact that the total number of actin waves is divided between the two neurites. We continue to use L_i for the neurite lengths in this system, though they are no longer random variables. Fig. 3B shows nullclines and the vector field for Eq. (5). There are seven equilibria, three of which are stable. Two correspond to the polarized state and are near the peaks of the probability distribution, while one near the origin corresponds to a state in which both neurites are short. The basin of attraction of the latter is small, so in the stochastic system described next trajectories leave this region quickly.

The bimodal probability density does not necessarily imply a firmly established axon. Monte Carlo simulations show that both neurite lengths alternate between two levels. That is, the system makes frequent transitions between the two polarized states (Fig. 3C). This is further indicated by the short mean transition time from one peak to

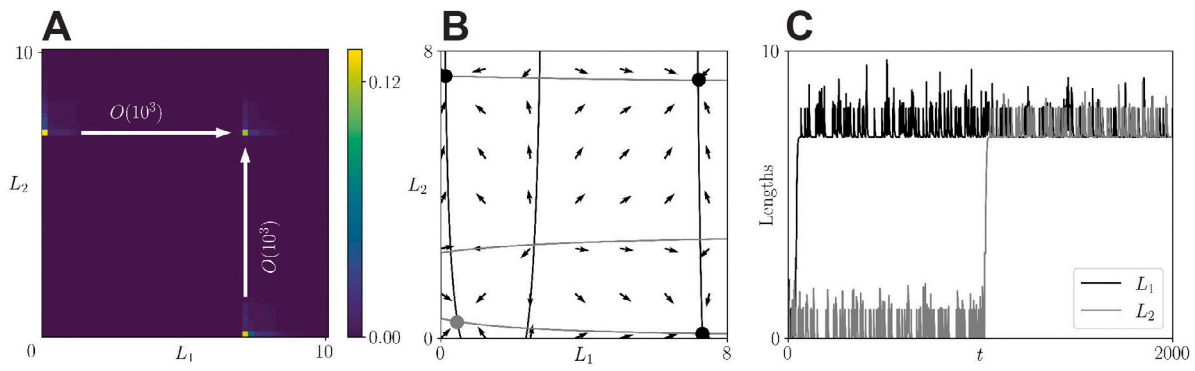

Fig. 4. The dynamics of the two-neurite system with negative feedback implemented through a length-dependent reduction in the excitation rate. (A) The probability density at $t = 400$ shows peaks at the two polarized states as well as a peak in which both neurites are long. The mean transition time from a polarized state to a nonpolarized state is $O(10^3)$ time units, estimated by the mean time to reach $[6, 10] \times [6, 10]$ from $(0, 8)$. (B) The phase portrait shows two stable equilibria at polarized states (black circles), another in which both neurites are short (gray), and another in which both are long (black). (C) A Monte Carlo simulation shows that both neurites become long at $t \approx 1000$. To study the effect of the excitation rate reduction alone, we set $r = r_0$ and $A = A_0$. Other parameter values are given in Table 1.

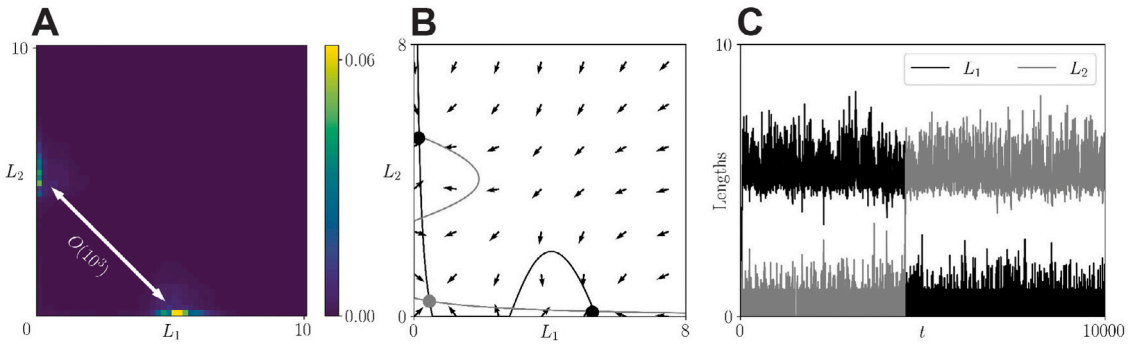

Fig. 5. The dynamics of the two-neurite system with negative feedback implemented through both a length-dependent increase in the retraction rate and a decrease in the excitation rate. (A) The long-term probability density is bimodal with two polarized states. The mean transition time between these states is $O(10^3)$. (B) The phase portrait shows two stable polarized equilibria and a stable equilibrium with small basin of attraction in which both neurites are short. (C) A Monte Carlo simulation shows the system flipping between the two polarized states. We set $\alpha = 0.02$ and $A = A_0$ here. Other parameter values are given in Table 1.

the other ($O(10^2)$ time units; see Fig. 3A). Thus, a single polarized state is not maintained when the negative feedback is implemented upon the retraction rate.

We next explore the dynamics in which negative feedback is implemented through length-dependent reduction in the excitation rate as prescribed by Eq. (3). The joint probability density initially has two peaks at the two polarized states. As time progresses, however, the polarized peaks fade and a third peak corresponding to two long neurites gains prominence (the top right peak in Fig. 4A). The mean transition time from a polarized state to the nonpolarized state is $O(10^3)$ time units (Fig. 4A). All three states appear as stable equilibria in the deterministic system, in addition to the stable equilibrium with a small basin of attraction corresponding to two short neurites (Fig. 4B). A Monte Carlo simulation shows the early development of a polarized state, followed by a transition to a state with two long neurites at $t \approx 1000$ (Fig. 4C). These results indicate that this form of negative feedback is not effective at maintaining a persistent polarized state. Incorporating both length-dependent increased retraction rate and reduced excitation rate eliminates the two long-neurite state (Fig. 5A and B), but does not prevent flipping between polarized states (Fig. 5C).

Finally, we consider negative feedback implemented through a length-dependent reduction in the excitation amplitude as prescribed by Eq. (4). Unlike the excitation rate reduction, the amplitude reduction yields a bimodal probability density that develops almost immediately (at $t = O(10)$, see Fig. 6A) and persists even at $t = 10^6$ (to be explained in the next section). A peak in which both neurites are long does not appear until much later, and the mean transition time from a polarized state to this nonpolarized state is $O(10^9)$ (Fig. 6B), which is much larger than the mean transition time when negative feedback is through rate reduction. Biologically, this means that the polarized state persists long enough that later stages of neuron development, including targeting of the nascent axon to appropriate targets via neurotrophins, can occur. Also, the system does not flip between the two polarized states, as shown with a Monte Carlo simulation (Fig. 6C). These results indicate that implementing negative feedback through a length-dependent reduction in the excitation amplitude results in persistent neuronal polarization.

4. Metastability resulting from different forms of negative feedback

We demonstrated above that regardless of the target of the negative feedback, the system enters a polarized state for some time before exiting to either (1) a different polarized state (i.e., flipping) or (2) a nonpolarized state (i.e., a state in which both neurites are long). However, the time that the system is in the polarized state varies greatly with the different forms of negative feedback. In this section, we examine why the persistence of the metastable polarized state is so different with the different negative feedback mechanisms. For this, we employ a tool called the ϵ-committor, developed by Lindner and Hellmann (2019). It provides an estimate of the probability that a stochastic trajectory remains in a region of phase space for a duration of $1/\epsilon$, where ϵ is the rate at which the trajectory is moved into an absorbing state connected to the region. A definition and description of the calculation of the ϵ-committor is given in the Appendix.

We focus on a region that encloses the upper left peak in any of the bimodal probability densities in the previous section: $R_S = [0, L_b] \times [L_b, L_{\max}]$ in the phase space (see the Appendix for the definition of

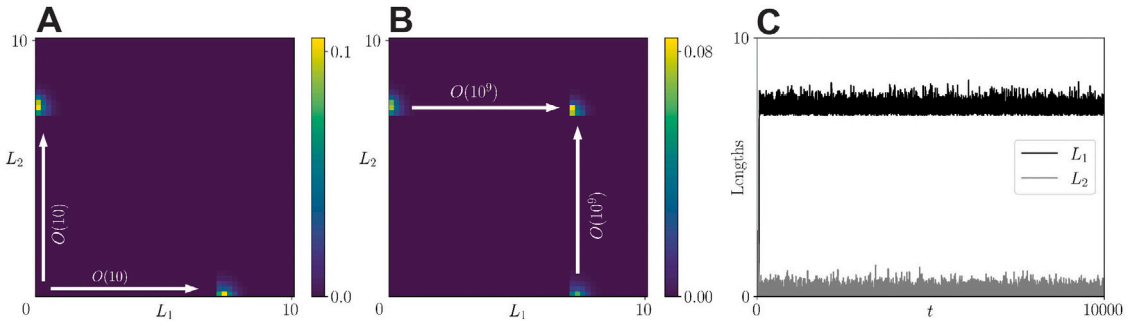

Fig. 6. The dynamics of the two-neurite system with negative feedback implemented through a length-dependent decrease in the excitation amplitude. (A) The probability density at $t = 10^6$ is bimodal. (B) The addition of another peak in the probability distribution occurs much later, after $O(10^9)$ time units. (C) A Monte-Carlo simulation shows a persistent polarized state. To study the effect of the excitation amplitude reduction alone, we set $r = r_0$ and $\lambda = \lambda_0$. Other parameter values are given in Table 1.

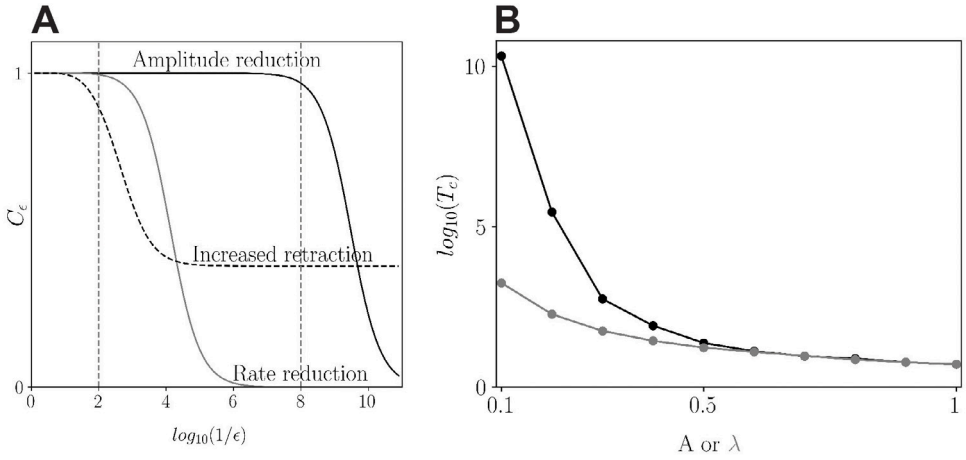

Fig. 7. Metastability resulting from different forms of negative feedback. (A) Strength of attraction of the polarized state S is measured by the ϵ-committor C_ϵ. Within the time window marked by the vertical dashed lines, C_ϵ is almost 1 when negative feedback is applied to the excitation amplitude, whereas it drops significantly when applied to the excitation rate or retraction rate. (B) The mean escape time T_c for a single neurite to surpass the threshold L_b increases faster when the excitation amplitude A is reduced (black) than when the excitation rate λ is reduced (gray).

$L_{\max}$). By definition, the ϵ-committor corresponding to R_S characterizes the persistence of the polarized state in which $L_2 \gg L_1$, for any of the three negative feedback mechanisms. Denote this ϵ-committor by C_ϵ. For each form of negative feedback, we calculate C_ϵ at different values of ϵ. Fig. 7A shows that when the negative feedback is on the excitation amplitude, $C_\epsilon \approx 1$ over a timescale of 10^8, meaning that with high probability a trajectory starting in R_S remains in R_S during this period of time. In contrast, C_ϵ falls to zero much earlier when the negative feedback is on the excitation rate. This indicates that the system leaves R_S quickly and explains the rapid transition from a bimodal probability density to a unimodal probability density corresponding to two long neurites (Fig. 4). C_ϵ starts to drop even earlier when the negative feedback is on the retraction rate, and it reaches ≈ 0.4. This means that the system spends about 40% of time in R_S in the long run, consistent with its flipping behavior. These ϵ-committorresults demonstrate again that applying the length-dependent negative feedback to the excitation amplitude works best in maintaining a unique polarized state.

The difference in the variations of C_ϵ when negative feedback is on excitation amplitude versus rate can also be quantified via the mean escape time. That is, the time at which a trajectory in a polarized state escapes to the other polarized state or to the nonpolarized state. Consider a single neurite of length L that follows Eq. (1). We use the general cell-mapping method (see the Appendix) to calculate the mean time that L, starting at $L = 0$, exceeds L_b for different values of A and λ (mimicking the effects of negative feedback on either of these two targets).

We find that the mean escape time (denoted by T_c) increases faster as the excitation amplitude is reduced than when rate is reduced (Fig. 7B). Therefore, reducing the excitation amplitude is more effective than reducing excitation rate on keeping a trajectory within an attracting basin. This explains the long persistence of the polarized state with negative feedback upon excitation amplitude.

Finally, we estimate the probability of crossing the threshold L_b starting from $L = 0$ for a single neurite. To overcome retraction, the neurite must receive at least L_b/A excitations during a short period (for simplicity, we assume that L_b/A is an integer here, which is true for the parameter values listed in Table 1. If L_b/A is not an integer, we need to round it up to the nearest integer. But this will not affect our result qualitatively). Consider $\tau = 1/r$, the timescale of retraction. Let P_c be the probability of having L_b/A excitations during τ, which follows a Poisson distribution:

$$P_c = \frac{(\lambda\tau)^{\frac{L_b}{A}} e^{-\lambda\tau}}{\left(\frac{L_b}{A}\right)!}. \tag{6}$$

With the Stirling's Approximation for factorial

$$n! = \sqrt{2\pi n}\left(\frac{n}{e}\right)^n, \tag{7}$$

we get

$$\ln(P_c) = \frac{L_b}{A}\left[\ln(\lambda\tau) - \ln\frac{L_b}{A} + 1\right] - \frac{1}{2}\ln\frac{L_b}{A} - \lambda\tau - \frac{1}{2}\ln(2\pi). \tag{8}$$

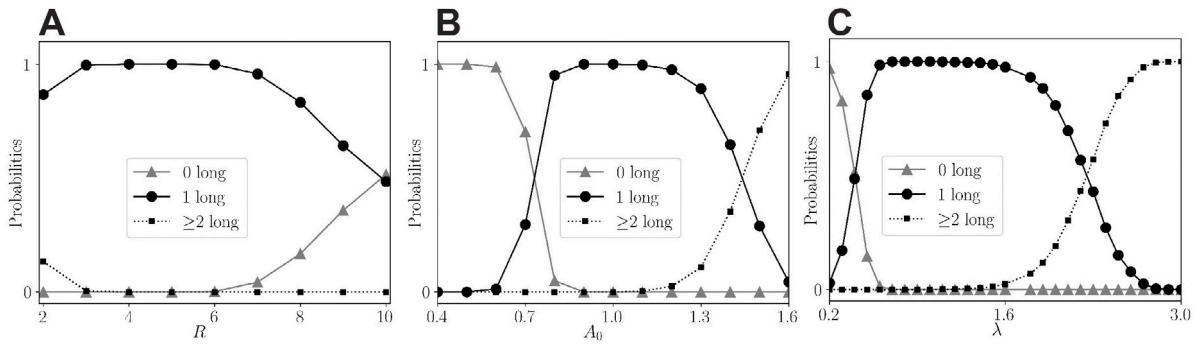

Fig. 8. Probabilities of having 0, 1 and ≥ 2 long neurites when the negative feedback is targeted to the excitation amplitude. (A) Varying neurite number R, with $A_0 = \lambda = 1$. (B) Varying base amplitude A_0, with $R = 4$ and $\lambda = 1$. (C) Varying excitation rate λ, with $R = 4$ and $A_0 = 1$. Each probability is obtained by running 2000 Monte Carlo simulation trials up to time 10 000. For all simulations, $\phi = 0.1$ and other parameter values are as in Table 1.

If the amplitude A is reduced to A/m ($m > 1$) and λ remains unchanged, then

$$\ln(P_c) = m\frac{L_b}{A}\left[\ln(\lambda\tau) + 1 - \ln\frac{L_b}{A} - \ln(m)\right] - \frac{1}{2}\ln\frac{L_b}{A} - \frac{1}{2}\ln(m) - \lambda\tau\frac{1}{2}\ln(2\pi). \tag{9}$$

Thus, $\ln(P_c)$ decreases faster than linear reduction. To see this more clearly, we plug in the parameter values in Table 1, namely $L_b = 3$, $A = 1$, $\lambda = 1$, $\tau = 1/r = 1$, and get

$$\begin{aligned}\ln(P_c) &= 3m[1 - \ln(3) - \ln(m)] - \frac{1}{2}\ln(m) - \frac{1}{2}\ln(3) - \frac{1}{2}\ln(2\pi) - 1 \\ &\sim -3m\ln(m), \qquad \text{for large } m.\end{aligned} \tag{10}$$

On the other hand, if A is unchanged and λ is reduced to λ/m ($m > 1$), then

$$\ln(P_c) = -\frac{L_b}{A}\ln(m) + \frac{L_b}{A}\ln(\lambda\tau) - \frac{\lambda\tau}{m} - \frac{L_b}{A}(\ln\frac{L_b}{A} - 1) - \frac{L_b}{A} - \frac{1}{2}\ln(2\pi). \tag{11}$$

With the parameter values mentioned above, we get

$$\begin{aligned}\ln(P_c) &= -3\ln(m) - \frac{1}{m} - 3(\ln(3) - 1) - \frac{1}{2}\ln(3) - \frac{1}{2}\ln(2\pi) \\ &\sim -3\ln(m), \qquad \text{for large } m,\end{aligned} \tag{12}$$

where we can see that $\ln(P_c)$ decreases with m logarithmically. Thus, the probability of crossing the threshold is much larger at small excitation rate compared with the probability at a small excitation amplitude. One can conclude from this that the persistence in a single polarized state is greater when negative feedback is applied to excitation amplitude.

5. Polarization with more than two neurites

Most developing neurons have between 2 and 10 neurites (Wissner-Gross et al., 2013). We next focus on the most effective form of negative feedback, targeted to the excitation amplitude, in model systems with more than 2 neurites. Results are obtained through Monte Carlo simulations, since the GCM approach to obtaining probability distributions is computationally expensive at higher dimensions. We seek to determine how the number of neurites R, as well as excitation amplitude and frequency, impact the probability of obtaining a single persistent polarized state.

The first set of results shows that the probability of obtaining a persistent polarized state first rises and then falls with the number of neurites, and the probability is almost 1 when R is from 3 to 6 (Fig. 8A). Within this range, the probabilities of having a state with 0 or ≥2 long neurites is almost zero. At smaller values of R, the probability of having ≥2 long neurites increases. In this case the actin waves are distributed among a smaller number of neurites, so that each receives more excitation that can push it across the threshold from short to long. At larger R values the probability of having no long neurites increases, since each neurite receives fewer actin waves and thus it becomes more likely that none will go past the threshold.

When the number of neurites is held constant at $R = 4$, an optimal range of parameter values exists for either the basal excitation amplitude or the excitation rate (Fig. 8B and C). If either parameter is too small, then the size or frequency of actin waves are too small for any of the neurites to cross over from small to long. If either parameter is too large, then more than one neurite will cross over despite of the negative feedback. The optimum range for all three parameters, R, A_0, and λ depend on the values of other parameter, as they are determined by the balance among excitatory pulses, retraction, and negative feedback. A change in the value of any one parameter changes the balance.

6. Bistability and excitation amplitude reduction in a limited-resource model

There have been several modeling studies in which the biophysical mechanism underlying neuronal polarization was competition for a limited supply of some growth factor or structural protein; the neurite acquiring the most becomes an axon (Hentschel et al., 1998; Naoki et al., 2011; Toriyama et al., 2010; Fivaz et al., 2008). In this section, we show how bistability and excitation amplitude reduction are involved in this mechanism.

To illustrate, we build a simple model based on (Toriyama et al., 2010). Consider a neuron with two neurites whose growth is supported by some growth factor F produced at the cell body. F is transported by actin waves to the neurite tips and diffuses back to the cell body. As in Toriyama et al. (2010), we assume that F slows down the retraction of the neurites. Let C_0, C_1 and C_2 be the concentrations of F at the cell body and the neurite tips. These quantities, and neurite lengths L_i, evolve according to:

$$\frac{\mathrm{d}C_i}{\mathrm{d}t} = -\frac{C_i - C_0}{aL_i} + B\sum_j \delta(t - t_j^{(i)}(\lambda)), \tag{13}$$

$$\frac{\mathrm{d}L_i}{\mathrm{d}t} = b - r_a(L_1 + L_2) - r_b\frac{K_c^5}{K_c^5 + C_i^5}\frac{L_i}{L_i + G}. \tag{14}$$

The first term on the right-hand side of Eq. (13) describes the Fickian flux of F which is proportional to the concentration gradient $(C_i - C_0)/L_i$. Unlike (Toriyama et al., 2010), we assume that C_0 is constant, so that the total amount of F is not conserved. (The results below are similar whether the growth factor is conserved or not.) The second term represents actin waves carrying the growth factor F. The term approximates the narrow Guassian spikes used in the original model (Toriyama et al., 2010). Each wave causes a jump of size B in concentration. The first two terms of Eq. (14) describe the growth of a neurite that is limited by a common resource that is used up as the neurites become longer (e.g., the protein tubulin, which is a key constituent of microtubules). The third term is the retraction rate that

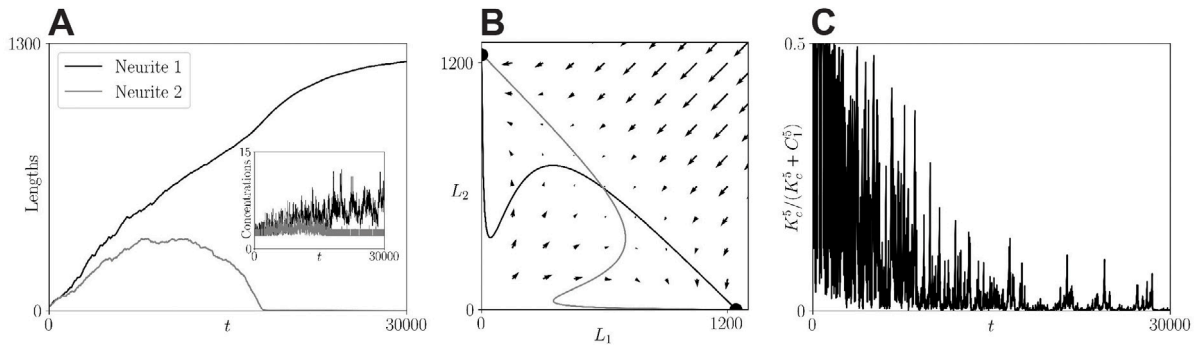

Fig. 9. Neuronal polarization with a limited-resource model. (A) A Monte Carlo simulation reproduces the emergence of a single axon. The inset shows the time evolution of the concentrations of the growth factor at two neurite tips. (B) The reduced two-dimensional system shows two stable equilibria (black filled circles). (C) For the neurite that develops into the axon (neurite 1), the fluctuation in its retraction rate, represented by $K_c^5/(K_c^5+C_1^5)$, becomes smaller as the neurite grows over time. Parameter values for these results are given in Table 2.

Table 2
List of parameters in the limited-resource model. We choose a constant excitation amplitude ($B = 1$), reflecting a constant level of growth factor at the cell body ($C_0 = 2$). Other parameter values are as in Toriyama et al. (2010).

Notation	Definition	Value
a	Diffusion parameter	0.121
B	Excitation amplitude	1*
λ	Excitation rate	0.059
b	Maximum growth rate	0.25
r_a	Fixed retraction rate	0.0002
r_b	Maximum fluctuating retraction rate	0.5
K_c	Half activation level	2
C_0	Concentration at the cell body	2

is reduced when growth factor is present. It retains the key properties of the original retraction term in the model in Toriyama et al. (2010): (1) the sharp reduction in the retraction rate as C_i gets closer to K_c; (2) the sigmoidal increase of the retraction rate with L_i.

Using parameter values based on experimental measurements in Toriyama et al. (2010) (see Table 2), Monte Carlo simulations reproduce the emergence of a single axon (Fig. 9A). Although fluctuating, the factor mostly accumulates in the long neurite that ultimately becomes the axon. To see bistability in the model, we replace the pulse term in Eq. (13) by its average $B\lambda/2$ to obtain an auxiliary deterministic system:

$$\frac{dC_i}{dt} = -\frac{C_i - C_0}{aL_i} + \frac{B\lambda}{2}, \tag{15}$$

$$\frac{dL_i}{dt} = b - r_a(L_1 + L_2) - r_b \frac{K_c^5}{K_c^5 + C_i^5}\frac{L_i}{L_i + G}. \tag{16}$$

This system evolves on two disparate time scales, with the growth factor concentrations changing much more rapidly than the neurite lengths. In the quasi-steady state, in which $dC_i/dt = 0$, C_i is given by

$$C_i = C_0 + \frac{B\lambda a L_i}{2}. \tag{17}$$

Substituting this expression for C_i into Eq. (16), we get a two-dimensional system for L_1 and L_2, whose phase portrait is shown in Fig. 9B. The two stable equilibria in the phase plane demonstrate the bistability in the model at the two polarized states.

To see that the model employs length-dependent excitation amplitude reduction, we plot $K_c^5/(K_c^5 + C_i^5)$ for the neurite that developed into the axon ($i = 1$ for the case shown in Fig. 9A), which provides for random fluctuation in its retraction rate. As Fig. 9C shows, the fluctuation becomes progressively smaller as the neurite grows. As a result, the "stochasticity" in the neurite length is damped as the neurite grows, reflecting an excitation amplitude reduction. Physically, the decay of the fluctuation results from the decreasing Fickian flux as the neurite grows, which facilitates growth factor accumulation. Length-dependent Fickian flux was also involved in other limited-resource models (Naoki et al., 2011; Hentschel et al., 1998).

In the original model (Toriyama et al., 2010), the total amount of the growth factor was assumed to be conserved. Therefore, the neurites competed for both the growth factor and structural proteins. Also, the excitation amplitude B was assumed to be proportional to C_0, which decreased as the neurites grew. This was a second means of reduction in the size of the stochasticity. Although unnecessary for successful neuronal polarization, as we showed here, these additional mechanisms may help the establishment of a single-axon in a noisy biological environment. Redundancy in biological processes is common in biological systems (Alon, 2020).

7. Discussion

In this article, we developed and analyzed a minimal model for achieving neuronal polarization that is based on what we believe to be the two key ingredients of the polarization process: bistability and length-dependent negative feedback. The bistability is necessary for the formation of two distinct classes of neurites (short and long), while the length-dependent negative feedback assures that once a neurite becomes long the others are prohibited from doing so. While there are several plausible targets of the negative feedback in the minimal model, we demonstrated that one stands out as the most effective in achieving persistent polarization. The success of this mechanism, targeted to the amplitude of stochastic actin waves, was demonstrated in several ways, including the joint probability distribution, Monte Carlo simulations, a large ϵ-committor, a long escape time from a polarized state, and a low escape probability. Additionally, we found that with this negative feedback mechanism, polarization is more successful if there are more than two neurites competing in the winner-takes-all contest. Finally, we demonstrated that a neuronal polarization model based on competition for a limited growth factor has the same underlying key ingredients as our most successful minimal model: bistability and length-dependent reduction in the excitation magnitude.

The clear distinctions between the axon and other short neurites of a neuron during its polarization indicate an inherent bistability (Dotti et al., 1988; Lamoureux et al., 2002). Typically, bistability arises from positive feedback (Alon, 2020), and various sources of positive feedback have been identified. One example involves length-dependent retrograde diffusion flux of polarity effectors (Toriyama et al., 2010; Naoki et al., 2011; Takano et al., 2017a). Another results from the anterograde transportation of polarity effectors that is enhanced by their accumulation at neurite tips (Fivaz et al., 2008), possibly due to stabilization of microtubules (Gomis-Rüth et al., 2008). Microtubule stabilization was also shown to help the localization of endoplasmic reticulum tubules, which in turn enhanced the stabilization (Farías

et al., 2019). Some of the signaling pathways involved in polarization are discussed in Schelski and Bradke (2017), Yogev and Shen (2017), Namba et al. (2015) and Takano et al. (2019).

Another major element of positive feedback in neurite growth is the autocrine effects of neurotrophic factors such as Brain-Derived Neurotrophic Factor (BDNF) and neurotrophin-3 (NT-3). These factors are released by individual neurites and bind to receptors on the neurites, stimulating their growth. It has been shown that BDNF activation of its receptor TrkB not only promotes neurite growth, but provides positive feedback by promoting BDNF secretion (Cheng et al., 2011). The impact of the local neurotrophin secretion depends on the receptor density at the neurite tip, and it has been shown that neurotrophin binding to receptors recruits more receptors to the membrane, thus providing positive feedback in the response to the neurotrophin (Cheng et al., 2011; Adler et al., 2006).

Once an axon has formed, negative feedback mechanisms are necessary to prevent the formation of a second axon. In this study, we examined three different unbiased negative feedback mechanisms. Length-dependent increased retraction prevents the growth of a short neurite by destroying its bistability. This negative feedback may result from long-range signals emitted from neurite tips (Kandel et al., 2013), or from a competition for material proteins (Toriyama et al., 2010). We showed that this mechanism is successful in creating polarized states, but does not prevent flipping between the polarized states, which does not appear to occur in actual neurons. This demonstrates that maintenance of a unique polarized state depends on length-dependent suppression of random actin waves, at least in the case of unbiased negative feedback. It is certainly possible that some form of biased negative feedback occurs, in which only a long neurite can initiate the negative feedback. One example of this is with the neurotrophin NT-3. This growth factor can accumulate at a long neurite and initiate Ca^{2+} waves that travel from the neurite tip back to the cell body, activating the small GTPase RhoA that inhibits growth of all neurites (Takano et al., 2017b). Thus, a growth factor can contribute to neuronal polarization by both facilitating growth of a neurite exposed to it and by inhibiting the growth of competing neurites.

In addition to increased retraction, we also studied the effects of reducing excitation rate and magnitude. We found that reducing excitation rate was insufficient for preventing the formation of a second axon, while reducing excitation magnitude effectively maintained the polarization of our model neuron. It was observed in previous experiments that the frequency of actin waves (i.e., the average number of actin waves per unit time) and the net growth driven by a single actin wave both decreased after an axon had formed (Ruthel and Banker, 1999a). Our study suggests that the decrease in net growth is a more crucial factor in preventing the formation of a second axon.

Previous studies have proposed a mechanism in which all neurites compete for a limited amount of growth proteins, and the neurite that acquired the most becomes an axon (Toriyama et al., 2010; Schelski and Bradke, 2017). It was assumed that the axon's acquisition of these proteins was facilitated by active anterograde transportation and retrograde diffusion. Using a simplification of one such model (Toriyama et al., 2010), we demonstrated that this mechanism exhibits bistability and a length-dependent reduction in excitation magnitude. The excitation magnitude reduction results from the axon's decreased diffusion flux as it grows. Length-dependent diffusion flux is not the only means of preventing the redistribution of growth proteins. It is also possible that blockage occurs in the long neurites. This was demonstrated in a study showing a novel cytoskeletal mechanism in which a dampened retrograde microtubule network assists in the accumulation of Kinesin-1 in the neurite that becomes the axon (Burute et al., 2022). Similar to the effect of slow diffusion, the retrograde transportation of Kinesin-1 is reduced, which prevents its redistribution among all neurites.

Our model's bistability and reduction in excitation magnitude may not completely prevent the emergence of multiple axons, which could be considered a flaw. However, a previous experimental study found that a short neurite was able to develop into an axon when it was mechanically stretched, even after another axon had already formed (Lamoureux et al., 2002). Our model easily explains this result, as mechanical stretching can cause a neurite to surpass the threshold length, putting it into the basin of attraction of the higher stable equilibrium, regardless of whether another axon already exists. In contrast, a limited resource model that does not allow for more than one axon could not account for this experimental finding.

In a prior experimental study by Wissner–Gross et al. it was observed that neurons with varying numbers of neurites polarized synchronously (Wissner-Gross et al., 2013). The authors found that prior models based on competition for a limited resource (Toriyama et al., 2010; Samuels et al., 1996) failed to replicate this, but instead the polarization time increased with the number of neurites. However, if the amount of the limited resource was increased with the number of neurites, the polarization time was similar for model cells with different numbers of neurites. Indeed, they found that the levels of two polarity factors, Shootin1 and HRas, were both higher in neurons with more neurites. We find similar behavior with our models. In the minimal model (Eq. (1)), if the basal excitation amplitude A_0 is properly upregulated according to the neurite number, the time to polarize will be similar regardless of the number of neurites. Similarly, for our limited-resource model (Eqs. (13) and (14)), if the concentration of the growth factor at the cell body, C_0, is adjusted based on the neurite number, the time to polarize will remain unchanged. The Wissner–Gross study also found that the majority of rat hippocampal neurons grown in cell culture had between 5 and 7 neurites (Wissner-Gross et al., 2013), suggesting the existence of an optimal range for the number of neurites, as in our Fig. 8, and raising the possibility of a regulatory mechanisms for achieving polarization by modulating both the number of neurites and the levels of effectors.

CRediT authorship contribution statement

Fan Bai: Conceptualization, Methodology, Software, Writing – original draft. **Richard Bertram:** Conceptualization, Methodology, Writing – review & editing, Funding acquisition. **Bhargav R. Karamched:** Conceptualization, Methodology, Writing – review & editing.

Declaration of competing interest

The authors declare that they have no known competing financial interests or personal relationships that could have appeared to influence the work reported in this paper.

Acknowledgment

We thank Michael Lindner for helpful discussions. BRK would like to thank his parents, Parthasarathy and Usha Karamched, for their love and unending support.

Funding

This research was partially supported by the National Science Foundation, grant number DMS 1853342, to R. Bertram.

Appendix

A.1. The generalized cell-mapping method

The generalized cell-mapping method (GCM) is a numerical implementation of the transfer operator (also called the Perron–Frobenius

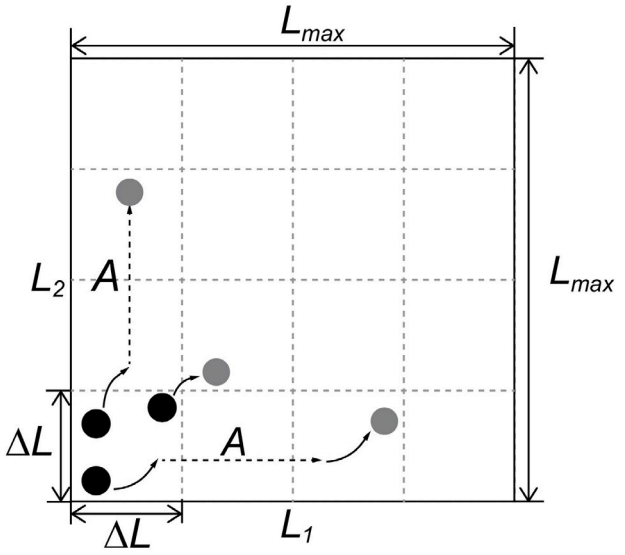

Fig. 10. Illustration of the generalized cell mapping method. The phase space of size $L_{\max} \times L_{\max}$ is divided into small square cells of size $\Delta L \times \Delta L$. Starting from a sample point, the two-neurite system may follow a continuous trajectory to reach another cell, or a discontinuous trajectory with a jump of size A in L_1 or L_2. The black and the gray dots mark the starting and ending positions, respectively. For purposes of illustration, the region is split into 4×4 cells. In actual simulations, we choose $\Delta L = 0.2$ and $L_{\max} = 10$, so that there are 50 cells in each direction. The time increment Δt to generate the trajectories is 0.1.

operator), often used to find the probability distributions of the quantities in a random dynamical system (Sun and Hsu, 1988; Wu and Zhu, 2008; Yue et al., 2012, 2013, 2019; Han et al., 2015). The GCM is also called Ulam's method (see Lindner and Hellmann (2019), Froyland (2001) and Froyland and Padberg (2009) and the references therein). The idea of the GCM is to discretize the system into a discrete-time Markov chain, and to calculate the distribution using the transition matrix. We use this method to compute probability distributions of neurite length.

To illustrate the method, consider a system of two neurites. We aim at finding the joint probability distribution $p(L_1, L_2, t)$ of neurite lengths, L_1 and L_2, at time t. We consider a region $[0, L_{\max}] \times [0, L_{\max}]$, where the upper bound $L_{\max}$ is large enough so that $p(L_1, L_2, t)$ is negligible outside the region. Then we divide the region into $N \times N$ square cells of width ΔL ($\Delta L = L_{\max}/N$), as shown in Fig. 10, and denote the cell in the ith row and jth column as $C_{i,j}$ ($i, j = 1, 2, \ldots, N$). To discretize time, we choose a small time increment Δt and only consider the distribution at $t = n\Delta t$ ($n = 0, 1, \ldots$). Then the probability that (L_1, L_2) falls within $C_{i,j}$ at $t = n\Delta t$, denoted by $p_{i,j}(n)$, is given by

$$p_{i,j}(n) = \Pr\{(L_1, L_2) \in C_{i,j} \text{ at } t = n\Delta t\} = \int_{(l_1,l_2)\in C_{i,j}} p(l_1, l_2, t)\, \mathrm{d}l_1 \mathrm{d}l_2, \quad (18)$$

where the notation $(l_1, l_2) \in C_{i,j}$ means that $l_1 \in [(i-1)\Delta L, i\Delta L]$ and $l_2 \in [(j-1)\Delta L, j\Delta L]$.

Let

$$\mathbf{p}(n) = (p_{1,1}(n), p_{1,2}(n), \ldots, p_{N,N}(n)) \quad (19)$$

be an 1-by-N^2 probability vector at time step n. Define the transition probability matrix $\mathbf{Q}$ as

$$\mathbf{Q} = \begin{bmatrix} Q_{(1,1)\to(1,1)} & Q_{(1,1)\to(1,2)} & \cdots & Q_{(1,1)\to(N,N)} \\ Q_{(1,2)\to(1,1)} & Q_{(1,2)\to(1,2)} & \cdots & Q_{(1,2)\to(N,N)} \\ \vdots & \vdots & \ddots & \vdots \\ Q_{(N,N)\to(1,1)} & Q_{(N,N)\to(1,2)} & \cdots & Q_{(N,N)\to(N,N)} \end{bmatrix} \quad (20)$$

where $Q_{(i',j')\to(i,j)}$ is the transition probability from $C_{(i',j')}$ to $C_{(i,j)}$ during Δt. (For our model, the Markov chain is time-independent, so $Q_{(i',j')\to(i,j)}$ does not depend on n). The probability vector at time step n is related to that at the previous time step by:

$$\mathbf{p}(n) = \mathbf{p}(n-1)\mathbf{Q}, \quad (21)$$

or

$$p_{i,j}(n) = \sum_{i',j'=1,2,\ldots,N} Q_{(i',j')\to(i,j)} p_{i,j}(n-1),$$
$$i, j = 1, 2, \ldots, N, \quad n = 1, 2, \ldots \quad (22)$$

To estimate $Q_{(i',j')\to(i,j)}$, we sample M points uniformly in $C_{(i',j')}$. Starting from each point, we could find a trajectory by solving Eq. (1) with a Monte Carlo method. Let $M_{i,j}$ be the number of trajectories that end in $C_{i,j}$, then $M_{i,j}/M$ approximates $Q_{(i',j')\to(i,j)}$. This should be repeated many times and the average taken. This is a time-consuming procedure, so we employ the more efficient procedure developed in Köylüoğlu et al. (1995). Starting from each sample point (i', j') we solve Eq. (1) without the stochastic term over time Δt:

$$\frac{\mathrm{d}L_i}{\mathrm{d}t} = g\,\frac{L_i^2}{L_i^2 + K^2} - rL_i, \quad i = 1, 2. \quad (23)$$

Let $M_{i,j}^{(d)}$ be the number of trajectories that end in $C_{i,j}$, then $M_{i,j}^{(d)}/M$ approximates the probability of transition from $C_{(i',j')}$ to $C_{i,j}$, provided no pulse occurs during Δt. (The superscript "(d)" represents "deterministic".) Then we consider the case where a single pulse occurs during Δt. Since we describe actin waves as a Poisson process, the time of the occurrence is uniformly distributed within Δt (Taylor and Karlin, 2010). Thus, we solve Eq. (23) over $\Delta t/2$, then randomly choose a length from L_1 and L_2 and add A to it, and finally solving Eq. (23) over the rest of the time interval $\Delta t/2$ (Fig. 10). The result is a trajectory with a single discontinuity. We repeat the same calculation for all sample points. Let $M_{i,j}^{(s)}$ be the number of trajectories that end in $C_{i,j}$, then $M_{i,j}^{(s)}/M$ approximates the probability of transition from $C_{(i',j')}$ to $C_{i,j}$, provided a single pulse occurs during this short period. (The superscript "(s)" represents "stochastic".) Since the probability of having two or more pulses during Δt is of $O(\Delta t^2)$, we neglect this probability and approximate $Q_{(i',j')\to(i,j)}$ as

$$Q_{(i',j')\to(i,j)} = (1 - \lambda\Delta t)\frac{M_{i,j}^{(d)}}{M} + \lambda\Delta t\,\frac{M_{i,j}^{(s)}}{M}, \quad (24)$$

where $\lambda\Delta t$ is the first order approximation of the probability of having a single pulse during Δt. In principle, one could refine the approximation by dividing Δt into more subintervals.

Given an initial distribution $\mathbf{p}(0)$, we can calculate $\mathbf{p}(n)$ iteratively with Eq. (21). To obtain $\mathbf{p}(0)$, suppose that the system starts from $(L_1(0), L_2(0))$. We find the cell $C_{i,j}$ containing this point and set the corresponding $p_{i,j}(0)$ to be 1 and all other probabilities to be 0. To estimate the limiting distribution $\mathbf{p}(\infty)$, we iterate according to Eq. (21), until the change in $\mathbf{p}(n)$ becomes negligible. To speed up the iteration, we utilize $\mathbf{Q}^{2^k} = (\mathbf{Q}^{2^{(k-1)}})^2$, such that $\mathbf{p}(2^k)$ can be obtained with k iterations.

In addition to solving the distribution, we will also use the GCM to calculate various first passage probabilities and mean first passage times. This requires modification of the transition matrix $\mathbf{Q}$. Suppose we are interested in finding the probability that the two-neurite system enters a specific region $\mathcal{D}$ and the mean entering time. For a cell centered within $\mathcal{D}$, the transition probability $Q_{(i',j')\to(i,j)}$ is modified as $\tilde{Q}_{(i',j')\to(i,j)}$:

$$\tilde{Q}_{(i',j')\to(i,j)} = \begin{cases} 1, & (i,j) = (i',j') \\ 0, & \text{otherwise} \end{cases} \quad (25)$$

This makes $\mathcal{D}$ an absorbing region, which means that once the system enters $\mathcal{D}$, it is frozen and cannot make further transitions. Let the modified transition matrix be $\tilde{\mathbf{Q}}$ and the resulting distribution be $\tilde{\mathbf{p}}(n)$. The probability of entering $\mathcal{D}$ at $t \le n\Delta t$ is given by

$$P_{\mathcal{D}}(n) = \sum_{C_{i,j}\in\mathcal{D}} \tilde{p}_{i,j}(n), \quad (26)$$

where $C_{i,j} \in D$ means that the center of $C_{i,j}$ is in D. The probability of entering D is given by

$$\Pr\{\text{Entering } D\} = P_D(\infty) = \sum_{C_{i,j}\in D} \tilde{p}_{i,j}(\infty), \tag{27}$$

which can be obtained by iterating enough number of times according to $\tilde{\mathbf{p}}(n) = \tilde{\mathbf{p}}(n-1)\tilde{\mathbf{Q}}$. Finally, let $\langle T_D\rangle$ be the mean entering time, then

$$\langle T_D\rangle = \sum_{n=1}^{\infty} n\Delta t(P_D(n) - P_D(n-1)). \tag{28}$$

Numerically, the series is truncated to drop the terms that make little contribution.

The GCM can be implemented regardless of the dimension of a system of interest. The mean escape time shown in Fig. 7B is calculated by applying the GCM to a single neurite. By setting $D = [L_b, L_{\max}]$, the mean T_c that the neurite length surpasses the threshold L_b is given by Eq. (28).

A.2. Monte Carlo simulations

In addition to the GCM, we also simulate the time evolution of the neurite lengths using a Monte Carlo method. The algorithm that we use is the following:

(1) Set the initial lengths $L_i(0) = 0$, $(i = 1, 2, \dots, R)$.
(2) At each time step $t = n\Delta t$, add to each $L_i(t)$ the deterministic increment $\Delta t[gL_i^2/(L_i^2 + K^2) - rL_i]$.
(3) Generate a random number u within $[0, 1]$. If $u > \lambda\Delta t$, go back to Step (2). Note that λ may be variable if there is length-dependent rate reduction (Eq. (3)).
(4) If $u \le \lambda\Delta t$, randomly choose an $L_i(t)$ from the N lengths, and add A to it. Note that A may be variable if there is length-dependent amplitude reduction (Eq. (4)). Then go back to Step (2).
(5) Repeat Steps (2) to (4) until iterations are completed.

We choose $\Delta t = 0.1$ for all simulations. The duration of a simulation depends on the type of negative feedback. Monte Carlo simulation is also applied to the winner-takes-all model (Eqs. (13) and (14)), and the implementation is similar.

A.3. Implementation of the ϵ-committor method

The ϵ-committor was introduced by Lindner and Hellmann (2019) as a means of estimating the probability that a stochastic trajectory remains in a region of phase space for a duration of $1/\epsilon$. Here, we describe its implementation within the framework of the GCM.

Consider the polarized state where $L_1 \ll L_2$, referred to as S in the following. To study its persistence, we choose a rectangular region $\mathcal{R}_S = [0, L_b] \times [L_b, L_{\max}]$, where L_b is the aforementioned location of the potential barrier and $L_{\max}$ is the user-defined boundary of the phase space in both directions. With the parameter values in Table 1, we have $L_b = 3$. The top-left peak of the bimodal probability density resulting from any of the negative feedback mechanisms described above (see Figs. 3, 4 and 6) falls into $\mathcal{R}_S$. Now we introduce two auxiliary absorbing states Z_1 and Z_2. When the system is in $\mathcal{R}_S$, it has a probability ϵ of being absorbed into Z_1 at each time step. When the system is in the rest of the region, it is absorbed into Z_2 at each time step with the same probability (Fig. 11). Let $q_{i,j}$ be the probability of being absorbed into Z_1 when the system starts from (the center of) $C_{i,j}$. The probability vector $\mathbf{q}$ formed by all $q_{i,j}$'s is called the ϵ-committor, namely

$$\mathbf{q} = (q_{1,1}, q_{1,2}, \dots, q_{N,N})^T. \tag{29}$$

Since the probability of being absorbed at each time step by either Z_1 or Z_2 is ϵ, the mean time till absorption is $\Delta t/\epsilon$, where Δt is the step size used in the GCM. Over such a timescale, if the system starts from $C_{i,j}$ and spends most of the time within $\mathcal{R}_S$, it will have a high probability of being absorbed into Z_1, i.e., $q_{i,j}$ will be close to 1. Conversely, if the system never enters $\mathcal{R}_S$ or quickly leaves it without coming back, $q_{i,j}$ will be close to 0 (Lindner and Hellmann, 2019). Therefore, $q_{i,j}$ characterizes the attracting strength of the region $\mathcal{R}_S$ over a timescale of $\Delta t/\epsilon$, when the system starts from $C_{i,j}$. By choosing a starting cell close to the top left peak of a bimodal distribution and changing the value of ϵ, the resulting $q_{i,j}$ quantifies the persistence of the polarized state S over different timescales under the corresponding negative feedback mechanism. Specifically, we choose the cell at $[0, 6]$ when the increased retraction is implemented, and the cell at $[0, 7]$ when the excitation rate or amplitude reduction is implemented. The corresponding probability $q_{i,j}(\mathcal{R}_S, \epsilon)$ is denoted by C_ϵ for notational simplicity.

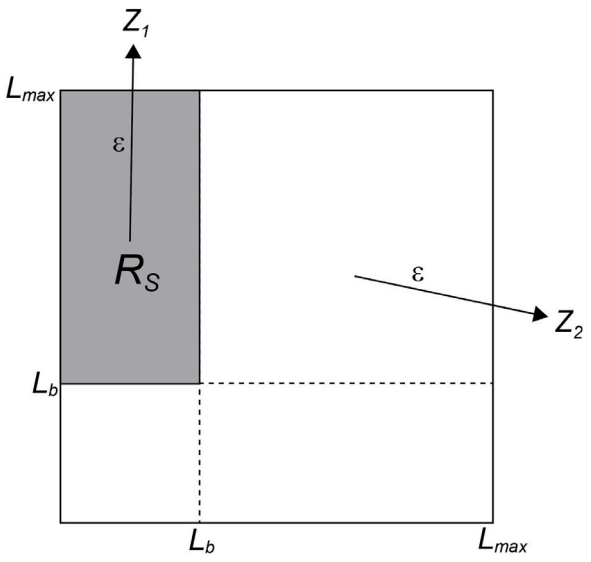

Fig. 11. Illustration of the ϵ-committor. Two absorbing states, Z_1 and Z_2 are introduced. When the system wanders within R_S (gray rectangle covering $[0, L_b]\times[L_b, L_{\max}]$), it has a probability of being absorbed into Z_1 at each time step. If the system is outside R_S, it has the same probability of being absorbed into Z_2.

To calculate $\mathbf{q}$ use the formula in Lindner and Hellmann (2019), given as

$$[\mathbf{I} - (1-\epsilon)\mathbf{Q}]\,\mathbf{q} = \epsilon\mathbf{I}_{\mathcal{R}_S}, \tag{30}$$

where $\mathbf{I}$ is an N^2-by-N^2 identity matrix and $\mathbf{Q}$ the transition matrix given by Eq. (20). $\mathbf{I}_{\mathcal{R}_S}$ is an N^2-by-1 indicator vector defined as

$$\mathbf{I}_{\mathcal{R}_S} = (\delta_{(1,1),\mathcal{R}_S}, \delta_{(1,2),\mathcal{R}_S}, \dots, \delta_{(N,N),\mathcal{R}_S})^T, \tag{31}$$

where

$$\delta_{(i,j),\mathcal{R}_S} = \begin{cases} 1, & (i,j) \in \mathcal{R}_S, \\ 0, & (i,j) \notin \mathcal{R}_S. \end{cases} \tag{32}$$

References

Adler, C.E., Fetter, R.D., Bargmann, C.I., 2006. UNC-6/Netrin induces neuronal asymmetry and defines the site of axon formation. Nature Neurosci. 9, 511–518.
Alon, Uri, 2020. An Introduction to Systems Biology. Taylor & Francis Group.
Arimura, N., Kaibuchi, K., 2007. Neuronal polarity: from extracellular signals to intracellular mechanisms. Nat. Rev. Neurosci. 8, 194–205.
Banker, G., 2018. The development of neuronal polarity: a retrospective view. J. Neurosci. 38, 1867–1873.
Burute, Mithila, Jansen, Klara I., Mihajlovic, Marko, Vermonden, Tina, Kapitein, Lukas C., 2022. Local changes in microtubule network mobility instruct neuronal polarization and axon specification. Sci. Adv. 8 (44), eabo2343.
Cheng, P.-L., Song, A.-H., Wong, Y.-H., Wang, S., Zhang, X., Poo, M.-M., 2011. Self-amplifying autocrine actions of BDNF in axon development. Proc. Natl. Acad. Sci. 108, 18430–18435.

Dotti, C.G., Sullivan, C.A., Banker, G.A., 1988. The establishment of polarity by hippocampal neurons in culture. J. Neurosci. 8 (4), 1454–1468.
Farías, Ginny G., Fréal, Amélie, Tortosa, Elena, Stucchi, Riccardo, Pan, Xingxiu, Portegies, Sybren, Will, Lena, Altelaar, Maarten, Hoogenraad, Casper C., 2019. Feedback-driven mechanisms between microtubules and the endoplasmic reticulum instruct neuronal polarity. Neuron 102 (1), 184–201.e8.
Fivaz, Marc, Bandara, Samuel, Inoue, Takanari, Meyer, Tobias, 2008. Robust neuronal symmetry breaking by ras-triggered local positive feedback. Curr. Biol. 18 (1), 44–50.
Froyland, Gary, 2001. In: Mees, Alistair I. (Ed.), Extracting Dynamical Behavior via Markov Models. Birkhäuser Boston, Boston, MA, pp. 281–321.
Froyland, Gary, Padberg, Kathrin, 2009. Almost-invariant sets and invariant manifolds — Connecting probabilistic and geometric descriptions of coherent structures in flows. Physica D 238 (16), 1507–1523.
Gomis-Rüth, Susana, Wierenga, Corette J., Bradke, Frank, 2008. Plasticity of polarization: Changing dendrites into axons in neurons integrated in neuronal circuits. Curr. Biol. 18 (13), 992–1000.
Goslin, K., Banker, G., 1989. Experimental observations on the development of polarity by hippocampal neurons in culture. J. Cell Biol. 108, 1507–1516.
Han, Qun, Xu, Wei, Yue, Xiaole, Zhang, Ying, 2015. First-passage time statistics in a bistable system subject to Poisson white noise by the generalized cell mapping method. Commun. Nonlinear Sci. Numer. Simul. 23 (1), 220–228.
Hentschel, H.G.E., Samuels, D., Fine, A., 1998. Instabilities during the dendritic and axonal development of neuronal form. Phys. A 254 (1), 46–61.
Inagaki, Naoyuki, Katsuno, Hiroko, 2017a. Actin waves: Origin of cell polarization and migration? Trends Cell Biol. 27 (7), 515–526.
Inagaki, Naoyuki, Katsuno, Hiroko, 2017b. Actin waves: Origin of cell polarization and migration? Trends Cell Biol. 27, 515–526.
Inagaki, N., Toriyama, M., Sakumura, Y., 2011. Systems biology of symmetry breaking during neuronal polarity formation. Dev. Neurobiol. 71, 584–593.
Kandel, Eric R, Schwartz, James H, Jessell, Thomas M, Siegelbaum, Steven A, Hudspeth, A J (Eds.), 2013. Principles of Neural Science. McGraw-Hill.
Köylüoğlu, Hasan Uğur, Nielsen, Søren R.K., Iwankiewicz, Radoslaw, 1995. Response and reliability of Poisson-driven systems by path integration. J. Eng. Mech. 121 (1), 117–130.
Lamoureux, Phillip, Ruthel, Gordon, Buxbaum, Robert E., Heidemann, Steven R., 2002. Mechanical tension can specify axonal fate in hippocampal neurons. J. Cell Biol. 159 (3), 499–508.
Lindner, Michael, Hellmann, Frank, 2019. Stochastic basins of attraction and generalized committor functions. Phys. Rev. E 100, 022124.
Namba, Takashi, Funahashi, Yasuhiro, Nakamuta, Shinichi, Xu, Chundi, Takano, Tetsuya, Kaibuchi, Kozo, 2015. Extracellular and intracellular signaling for neuronal polarity. Physiol. Rev. 95 (3), 995–1024, PMID: 26133936.
Naoki, Honda, Ishii, Shin, 2014. Chapter six - mathematical modeling of neuronal polarization during development. In: Blackwell, Kim T. (Ed.), Computational Neuroscience. In: Progress in Molecular Biology and Translational Science, vol. 123, Academic Press, pp. 127–141.
Naoki, Honda, Nakamuta, Shinichi, Kaibuchi, Kozo, Ishii, Shin, 2011. Flexible search for single-axon morphology during neuronal spontaneous polarization. PLOS ONE 6 (4), 1–9.
Noctor, S.C., Martinez-Cereno, V., Ivic, I., Kriegstein, A.R., 2004. Cortical neurons arise in symmetric and asymmetric division zones and migrate through specific phases. Nature Neurosci. 7, 136–144.
Ruthel, Gordon, Banker, Gary, 1999a. Role of moving growth cone–like "wave" structures in the outgrowth of cultured hippocampal axons and dendrites. J. Neurobiol. 39 (1), 97–106.
Ruthel, Gordon, Banker, Gary, 1999b. Role of moving growth cone–like "wave" structures in the outgrowth of cultured hippocampal axons and dendrites. J. Neurobiol. 39, 97–106.
Samuels, David C., Hentschel, H.G.E., Fine, Alan, 1996. The origin of neuronal polarization: a model of axon formation. Philos. Trans. R. Soc. Lond. Ser. B 351 (1344), 1147–1156.
Schelski, Max, Bradke, Frank, 2017. Neuronal polarization: From spatiotemporal signaling to cytoskeletal dynamics. Mol. Cell. Neurosci. 84, 11–28, Cytoskeleton-dependent regulation of neuronal network formation.
Sun, J.-Q., Hsu, C.S., 1988. First-passage time probability of non-linear stochastic systems by generalized cell mapping method. J. Sound Vib. 124 (2), 233–248.
Tabata, H., Nakajima, K., 2003. Multipolar migration: the third mode of radial neuronal migration in the developing cerebral cortex. J. Neurosci. 23, 9996–10001.
Takano, Tetsuya, Funahashi, Yasuhiro, Kaibuchi, Kozo, 2019. Neuronal polarity: Positive and negative feedback signals. Front. Cell Dev. Biol. 7, 69.
Takano, Tetsuya, Wu, Mengya, Nakamuta, Shinichi, Naoki, Honda, Ishizawa, Naruki, Namba, Takashi, Watanabe, Takashi, Xu, Chundi, Hamaguchi, Tomonari, Yura, Yoshimitsu, Amano, Mutsuki, Hahn, Klaus M., Kaibuchi, Kozo, 2017a. Discovery of long-range inhibitory signaling to ensure single axon formation. Nature Commun. 8 (1), 33.
Takano, Tetsuya, Wu, Mengya, Nakamuta, Shinichi, Naoki, Honda, Ishizawa, Naruki, Namba, Takashi, Watanabe, Takashi, Xu, Chundi, Hamaguchi, Tomonari, Yura, Yoshimitsu, Amano, Mutsuki, Hahn, Klaus M., Kaibuchi, Kozo, 2017b. Discovery of long-range inhibitory signaling to ensure single axon formation. Nat. Comm. 8, 33.
Taylor, Howard M., Karlin, Samuel, 2010. An Introduction to Stochastic Modeling. Academic Press.
Toriyama, Michinori, Sakumura, Yuichi, Shimada, Tadayuki, Ishii, Shin, Inagaki, Naoyuki, 2010. A diffusion-based neurite length-sensing mechanism involved in neuronal symmetry breaking. Mol. Syst. Biol. 6 (1), 394.
Winans, Amy M., Collins, Sean R., Meyer, Tobias, 2016. Waves of actin and microtubule polymerization drive microtubule-based transport and neurite growth before single axon formation. ELife 5, e12387.
Wissner-Gross, Zachary D., Scott, Mark A., Steinmeyer, Joseph D., Yanik, Mehmet Fatih, 2013. Synchronous symmetry breaking in neurons with different neurite counts. PLOS ONE 8 (2), 1–8.
Wu, Y., Zhu, W.Q., 2008. Stochastic analysis of a pulse-type prey-predator model. Phys. Rev. E 77, 041911.
Yamamoto, H., Demura, T., Morita, M., Banker, G.A., Tanli, T., Nakamura, S., 2012. Differential neurite outgrowth is required for axon specification by cultured hippocampal neurons. J. Neurochem. 123, 904–910.
Yogev, Shaul, Shen, Kang, 2017. Establishing neuronal polarity with environmental and intrinsic mechanisms. Neuron 96 (3), 638–650.
Yue, Xiaole, Xu, Wei, Jia, Wantao, Wang, Liang, 2013. Stochastic response of a $\phi 6$ oscillator subjected to combined harmonic and Poisson white noise excitations. Phys. A 392 (14), 2988–2998.
Yue, Xiaole, Xu, Wei, Wang, Liang, Zhou, Bingchang, 2012. Transient and steady-state responses in a self-sustained oscillator with harmonic and bounded noise excitations. Probab. Eng. Mech. 30, 70–76.
Yue, Xiaole, Xu, Wei, Xu, Yong, Sun, Jian-Qiao, 2019. Non-stationary response of MDOF dynamical systems under combined Gaussian and Poisson white noises by the generalized cell mapping method. Probab. Eng. Mech. 55, 102–108.